Manipulation of Nanoscale Phase Separation and Optical Properties of P3HT/PMMA Polymer Blends for Photoluminescent Electron Beam Resist

Ming-Chung Wu,[†,⊥] **Hsueh-Chung Liao,**[†,⊥] **Yi Chou,**[†] **Che-Pu Hsu,**[†] **Wei-Che Yen,**[‡]
Chih-Min Chuang,[§] **Yun-Yue Lin,**[†] **Chun-Wei Chen,**[†] **Yang-Fang Chen,**[*,‖] **and Wei-Fang Su**[*,†,‡]

Department of Materials Science and Engineering, National Taiwan University, Taipei 106-17, Taiwan; Institute of Polymer Science and Engineering, National Taiwan University, Taipei 106-17, Taiwan; Institute of Nuclear Energy Research, Atomic Energy Council, Taiyuan 325-46, Taiwan; and Department of Physics, National Taiwan University, Taipei 106-17, Taiwan

A novel photoluminescence electron beam resist made from the blend of poly(3-hexylthiophene) (P3HT) and poly(methyl methacrylate) (PMMA) has been successfully developed in this study. In order to optimize the resolution of the electron beam resist, the variations of nanophase separated morphology produced by differing blending ratios were examined carefully. Concave P3HT-rich island-like domains were observed in the thin film of the resist. The size of concave island-like domains decreased from 350 to 100 nm when decreasing the blending ratio of P3HT/PMMA from 1:5 to 1:50 or lower, concurrently accompanied by significant changes in optical properties and morphological behaviors. The λ_{max} of the film absorption is blue-shifted from 520 to 470 nm, and its λ_{max} of photoluminescence (PL) is also shifted from 660 to 550 nm. The radiative lifetime is shorter while the luminescence efficiency is higher when the P3HT/PMMA ratio decreases. These results are attributed to the quantum confinement effect of single P3HT chain isolated in PMMA matrix, which effectively suppresses the energy transfer between the well-separated polymer chains of P3HT. The factors affecting the resolution of the P3HT/PMMA electron beam resists were systematically investigated, including blending ratios and molecular weight. The photoluminescence resist with the best resolution was fabricated by using a molecular weight of 13 500 Da of P3HT and a blending ratio of 1:1000. Furthermore, high-resolution patterns can be obtained on both flat silicon wafers and rough substrates made from 20 nm Au nanoparticles self-assembled on APTMS (3-aminopropyltrimethoxysilane)-coated silicon wafers. Our newly developed electron beam resist provides a simple and convenient approach for the fabrication of nanoscale photoluminescent periodic arrays, which can underpin many optoelectronic applications awaiting future exploration.

1. Introduction

Electron beam lithography is a technique to generate patterns on a surface using a beam of electrons. Although the pattern generation rate appears slower than parallel techniques like photolithography, electron beam lithographic patterning can easily reach the nanoscale regime by controlling the electron beam width. Additionally, electron beam lithography can overcome the diffraction limit of light to write nanopatterns. Electron beam resists are usually passive and lack specific functions. If one can develop resists with active functions such as conductivity,[1−3] luminescence,[4,5] and magnetic properties,[6−10] the fabrication process of specific devices can be simplified. However, relatively few active resists has been reported. Pang et al. fabricated a PMMA/quantum dot (QD) composite photoluminescent resist, by first mixing methyl methacrylate and colloidal semiconductor QDs together and then polymerizing the mixture.[11] Nurmikko et al. reported nanoengineered fluorescence from an active resist composed of semiconductor core−shell (CdSe/ZnS) quantum dots, which are close to the surface plasmon polarization field of periodic Ag arrays.[12]

Previously, we adopted gold surface plasmons to enhance the emission of CdSe in Au-coated CdSe/PMMA periodic arrays.[13] However, since quantum dots are difficult to disperse evenly in a polymer matrix, the resolution of the photoluminescent electron beam resist is significantly affected by the compatibility between organic and inorganic materials. To resolve this difficulty, our new resist has an outstanding photoluminescent property and is well compatible with PMMA; this blend of conjugated polymer and PMMA thus provides an excellent potential for the application of active electron beam resists.

Conjugated polymers are frequently used in various fields including light-emitting electrochemical cells (LECs),[14−18] photovoltaic devices (PVs),[19] photodiodes,[20,21] transistors,[22,23] and lasers[24] due to the advantages of color tunability, good film-forming property, and superior flexibility as compared to inorganic semiconductors. In addition, the physical blending of polymers provides a simple, low-cost, and effective way to obtain novel materials for optoelectronic applications. For example, LEDs[16,25,26] and PVs based on a blend of conjugated polymers are more efficient than those based on single polymeric material because the phase separation in the blend can create a series of self-assembled heterojunctions where exciton dissociation (in a PV) or charge recombination (in an LED) can occur.[27] Regarding blends of conjugated polymers and nonconjugated polymers, their optical and morphological properties significantly varied with different blending ratios.[28,29] If the ratio of conjugated polymer to nonconjugated polymer in the blend is

---

* To whom correspondence should be addressed.
† Department of Materials Science and Engineering, National Taiwan University.
‡ Institute of Polymer Science and Engineering, National Taiwan University.
§ Atomic Energy Council.
‖ Department of Physics, National Taiwan University.
⊥ These authors contributed equally for this work.

high, the blend morphology is patterned with tens of micrometer-scale dots with no change in photoluminescence spectrum. When the ratio is small, microisolated dots in a nonconjugated matrix are formed. The dots emit light similar to pristine conjugated polymers, but the nonconjugated polymer matrix can also emit light with a blue shift of ~100 nm.[30]

In this study, we have developed a high-resolution photoluminescent electron beam resist using polymer blends consisting of the conjugated polymer poly(3-hexylthiophene) (P3HT) and a nonconjugated polymer poly(methyl methacrylate) (PMMA). The morphology, molecular weight, and optical properties that affect resolution by incorporating different blending ratios have been systematically studied. Our novel photoluminescent resist was successfully developed by simply blending a luminescent polymer and nonluminescent polymer. This is very useful for constructing high-resolution planar 2D photoluminescent arrays. Therefore, our resist opens up a new route for the application of optoelectronic devices.

2. Experimental Section

2.1. Synthesis and Characterization of Different Molecular Weight HT−HT Poly(3-hexylthiophene) (P3HT). P3HTs with different MWs were synthesized according to the literature[31] with some modifications. Typically, 2,5-dibromo-3-hexylthiophene (0.030 mol, 10 g) was added into a 500 mL three-neck round-bottom flask equipped with a 24/40 ground joint, a reflux condenser, and a magnetic stir bar. It was then purged with dry nitrogen for 15 min. 320 mL of freshly distilled THF was transferred to the flask, and the solution was stirred under dry nitrogen. A solution of *tert*-butylmagnesium chloride in diethyl ether (0.032 mol, 16 mL) was added via an airtight syringe and then heated for reflux for 1.5 h. The solution was allowed to cool to room temperature followed by the addition of Ni(dppp)Cl$_2$ and stirring at room temperature for 0.5 h. The solution was poured into methanol (500 mL). This action led to precipitation. The solid was collected in a cellulose extraction thimble and then washed with methanol in a Soxhlet apparatus. By changing the amount of Ni(dppp)Cl$_2$, P3HT samples with different MWs (13.5, 33.8, and 62.0 kDa) were obtained, representing low-, medium-, and high-MW samples, respectively. The polymer was dried under vacuum overnight and gathered as a dark purple material (60% yield). The MWs and polydispersity (PDI) values of the P3HTs were determined by gel permeation chromatography (GPC) on a Waters 1525 binary HPLC pump with polystyrene as standard and tetrahydrofuran (THF) as the solvent. The regiospecificity (RR) of P3HT was determined by the NMR spectroscopy using a Bruker AVANCE 400 spectrometer with CDCl$_3$ as solvent and tetramethylsilane as an internal standard.

2.2. Preparation of P3HT/PMMA Polymer Blend Thin Films. The 0.2 wt % P3HT and 2.0 wt % PMMA (Aldrich, MW ∼ 996 000) polymer solutions were prepared in chlorobenzene and stirred for 2 and 48 h at room temperature, respectively. The P3HT/PMMA blend solutions were obtained by mixing P3HT and PMMA solutions with different weight ratios, namely sample A, 1:5; sample B, 1:10; sample C, 1:50; sample D, 1:100; sample E, 1:500; and sample F, 1:1000, and then stirring them for 24 h at room temperature. These P3HT/PMMA blend solutions were spin-coated onto silicon wafers at 3000 rpm for 90 s to give a nominal thickness of ∼200 nm. Finally, the P3HT/PMMA thin films were baked at 180 °C for 10 min.

2.3. Fabrication of Au Nanoparticles Self-Assembled Substrate.[32−34] All chemicals were purchased and used as received without further purification. 30 mg of gold(III) chloride

trihydrate (HAuCl$_4$·3H$_2$O, Acros, 99.8%) was dissolved in 15.0 g of deionized water and heated to 100 °C while stirring vigorously. 10 mg of trisodium citrate dihydrate (C$_6$H$_5$Na$_3$O$_7$·2H$_2$O, Acros, 99%) in 0.8 mL of deionized water was then added and kept at 100 °C for 5 min. The reaction was cooled to room temperature and then diluted by deionized water to make a final product of 0.01 wt % ∼20 nm Au colloid solution.

The cleaned silicon substrates were immersed in a solution of 3-aminopropyltrimethoxysilane (APTMS, Acros, 97%)/deionized water/isopropyl alcohol with a volume ratio of (1:1: 40 v/v) for 24 h. After the immersion, the sample was cleaned by deionized water and baked at 120 °C for 2 h. The Au nanoparticles (diameter ∼20 nm) were assembled on the APTMS/silicon substrate surface by immersing the substrate into the Au colloid suspension for 12 h. The substrate was rinsed with deionized water immediately after removing from Au colloid suspension and was dried in the oven at 120 °C for 2 h.

2.4. P3HT/PMMA Nanopatterns Fabricated by Electron Beam Lithography. High-resolution nanolithography was performed by writing specific patterns across a 150 μm field with a 2.5 nm beam step size using a high-resolution electron beam lithography system, ELIONIX ELS-7000EX. The system provides a stable 1.8 nm electron beam using high beam currents at 100 keV. After the film was exposed to the electron beam, it was developed by using mixed solvents of methyl isobutyl ketone and isopropanol (25:75 by volume) for 40 s, then isopropanol for 20 s, and finally deionized water for 20 s.

2.5. Measurements. The surface morphology of our novel materials was examined by an atomic force microscope (AFM, Digital Instruments, Dimension-3100 Multimode) in tapping mode. Confocal Raman mapping measurements were conducted with the confocal microscope (WITec, CMR200, Germany) in the backscattering mode. Diffraction-limited confocal Raman microscopy gives a lateral spatial resolution (∼300 nm) of approximately half the excitation wavelength (λ_{exe} = 632.8 nm). The laser beam was focused with a 100× objective (Olympus, IX-70 (NA = 0.95)) making the laser focus beam ∼1.0 μm in diameter, which corresponds to three or four pixels in the integrated Raman image. The steady state PL spectra were obtained by pumping the samples with a continuous wave (CW) He−Cd laser (λ_{exe} = 325 nm), and the emission spectra were analyzed using a Jobin-Yvon Triax 0.55 m monochromator and detected by a photomultiplier tube and standard photon-counting electronics. Time-resolved photoluminescence spectroscopy was performed using a time-correlated single photon counting (TCSPC) spectrometer (Picoquant, Inc.). A pulse laser (λ_{exe} = 375 nm) with an average power of 1 mW, operating at 40 MHz, with duration of 70 ps was used for excitation. The photoluminescence distribution of P3HT/PMMA thin film was measured by confocal microscopy (WITec, AlphaSNOM, Germany). The Ar ion laser (λ_{exe} = 488 nm) was used to excite the thin film through a 100× Nikon plan objective (NA ∼ 0.9). A single photon counting photomultiplier tube detector was used to detect the fluorescence intensity.

3. Results and Discussion

In order to optimize the resolution of the resist, the control of the morphology of the P3HT/PMMA blend is extremely important. The distinct phase separation and island-like domain formation are clearly observed for different ratios of P3HT/PMMA films as shown in Figure 1. We can observe that the changes of blending ratio lead to the size alternation and depth variation of the island-like domains. The changes of miscibility
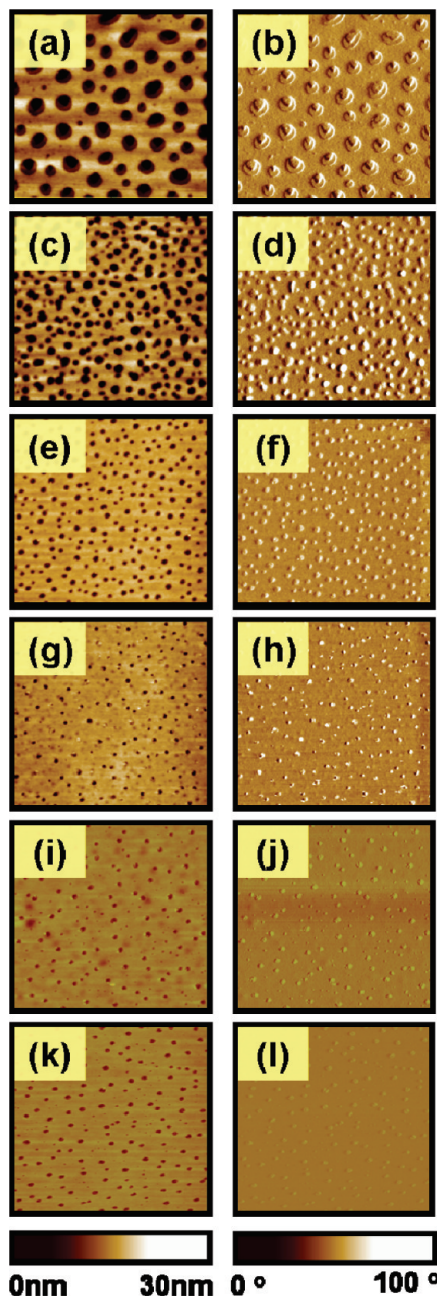
P3HT/PMMA Polymer Blends

J. Phys. Chem. B, Vol. 114, No. 32, 2010 **10279**

Figure 1. Tapping-mode AFM topographic (a, c, e, g, i, k) and phase shift images (b, d, f, h, j, l) of P3HT/PMMA blends with different P3HT concentrations (5 μm × 5 μm). The ratio of P3HT and PMMA are (a, b) sample A, 1:5; (c, d) sample B, 1:10; (e, f) sample C, 1:50; (g, h) sample D, 1:100; (i, j) sample E, 1:500; and (k, l) sample F, 1:1000.

Figure 2. Box chart depicting the concave island-like domains sizes on the surface of P3HT/PMMA thin films with different blending ratios.

TABLE 1: Compositions and Surface Properties of P3HT/PMMA Thin Films Containing Concave Island-like Domains

sample	blending ratio (P3HT/PMMA)	diameter of the island (av) (nm)	max depth of the island (av) (nm)	rms roughness (nm)
A	1:5	346 ± 91	15.5	4.01
B	1:10	143 ± 45	12.6	3.92
C	1:50	103 ± 27	9.7	1.72
D	1:100	98 ± 28	9.5	1.16
E	1:500	98 ± 30	9.3	0.76
F	1:1000	101 ± 28	9.4	0.78

(Table 1). Although the depth of concave domain would affect the morphology of P3HT/PMMA, it does not result in the obvious effect. Moreover, the average sizes and the numbers of the island-like domains become similar among the films with the blending ratios lower than 1:50, such as samples D, E, and F. Hence, the concentration of the P3HT chains in PMMA matrix decreases with decreasing P3HT/PMMA ratio for those samples of low blending ratios. It results the presence of the single P3HT chain in the PMMA phase of sample F (P3HT/PMMA ∼ 1:1000).

Raman spectroscopy can determine the chemical composition distribution of the phase separated domains in the blend of P3HT/PMMA. The P3HT exhibits prominent Raman bands of 1440 cm^{-1} (C=C stretching vibrations of the thiophene ring) and 1380 cm^{-1} (C−C skeletal stretching),[37] which is different from the characteristic C=O peak of PMMA at 2954 cm^{-1}.[38] We used a scanning confocal Raman microscope to obtain the Raman image of P3HT/PMMA (1:5 ratio) thin film by intensity integration of the spectral ranging from 1200 to 3500 cm^{-1} as shown in Figure 3a. High-intensity domains and low-intensity domains were observed, and they are labeled as region A and region B, respectively. By intensity integration of the spectrum ranging from 1350 to 1550 cm^{-1} that is specific for the P3HT component of the film, we observed that region A exhibits high intensity as shown in Figure 3b. This result indicates that region A is a P3HT-rich region. We further confirmed the results by intensity integration of the spectrum ranging from 2800 to 3100 cm^{-1} that is specific to the PMMA, and the bright regions of Figure 3b become dark as shown in Figure 3c. The exact chemical composition of each region can be deduced from its Raman spectrum. Indeed, region A is P3HT-rich (Figure 3d) while region B is PMMA-rich (Figure 3e) as compared to the spectra of pristine P3HT (Figure 3f) and pristine PMMA (Figure 3g).

It is well-known that the morphological variation can significantly affect the optical behavior of a blend film. Thus,

of two polymers system are according to the free energy of mixing, which depends on both enthalpy and entropy contributions of the system. For most of binary polymeric blends, the entropy of mixing is small, leaving the enthalpy factor to be the determinant.[35,36] Unfavorable enthalpy interaction in polymer blend leads to phase separation of the blends in both nanoscale and submicroscale. The phase-separated domains show different solvent evaporation rates which result in different surface profile. Figure 2 shows the analysis of size distribution for the concave island-like domains on the surface of P3HT/PMMA thin films with different blending ratios. Here the molecular weight of P3HT is kept at 13 500 g/mol. The average sizes of the island-like domains decrease from 350 nm (sample A) to 100 nm (sample C) with decreasing P3HT/PMMA ratio from 1:5 to 1:50
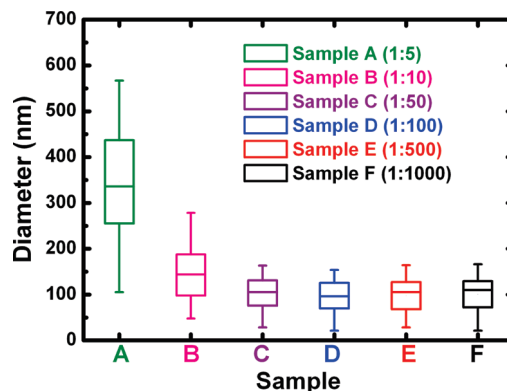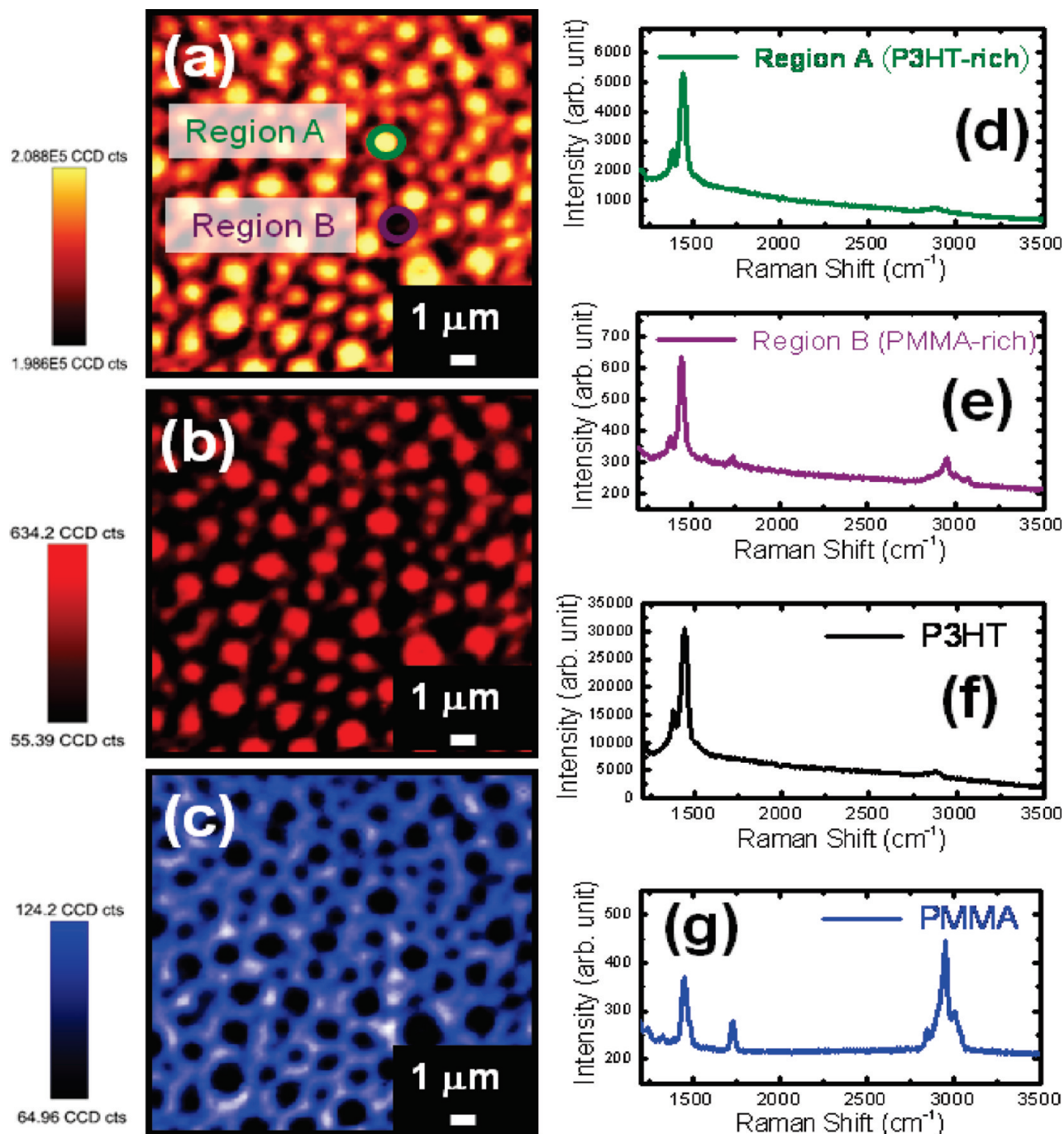
Figure 3. Confocal Raman mapping images of sample A (P3HT/PMMA blending ratio is 1:5) and Raman spectra of sample A, pristine P3HT and pristine PMMA. Raman mapping image that integrated the spectra from (a) 1200 to 3500 cm^{-1} (full spectra), (b) 1350 to 1550 cm^{-1} (P3HT Raman signals range), and (c) 2800 to 3100 cm^{-1} (PMMA Raman signals range). Raman spectra of (d) P3HT-rich region, (e) PMMA-rich region, (f) pristine P3HT, and (g) pristine PMMA.

we studied the optical properties of our blended resist. Figure 4 shows the UV−vis absorption spectra of P3HT/PMMA thin films with different blending ratios. The pristine P3HT sample with molecular weight of 13.5 kDa shows a λ_{max} absorption of 555 nm. When the P3HT concentration is high, the absorption of the films (samples A−D) exhibits a small blue shift to 525 nm. As the P3HT/PMMA ratio decreases, the absorption of the blend films of 1:500 (sample E) and 1:1000 (sample F) shows a large blue shift to 470 nm. The results indicate the P3HT is more isolated and less interactive in the samples of low P3HT/PMMA ratio as compared to the samples of high P3HT/PMMA ratio. The mechanism of the blue shift will be explained later in more detail.

Figure 5a,b shows the micro-photoluminescence (μ-PL) spectra and time-resolved photoluminescence (TRPL) of the films with different P3HT/PMMA ratios. We found out that both thin films of high ratios, sample A (1:5) and sample B (1:10), show a PL spectra peak around 660 nm, which is similar to that of pristine P3HT (Figure 5a). However, when the P3HT/PMMA ratio decreases, the peak at 660 nm shrinks gradually and finally vanishes while the signals of a new photolumines-cence peak around 550 nm becomes stronger. The micropho-toluminescence (μ-PL) spectra only show the overall PL of the films, so confocal microscopy was utilized to examine the photoluminescence distribution over the samples of different blending ratios as shown in Figure 6a−f. A more intense,
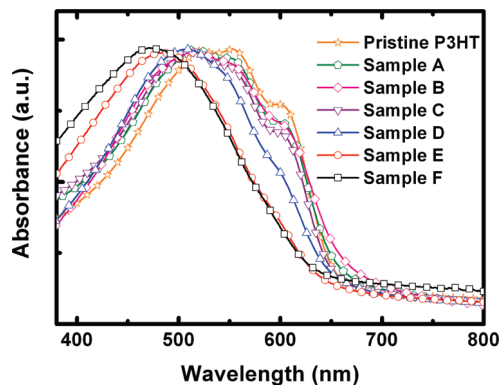
P3HT/PMMA Polymer Blends

J. Phys. Chem. B, Vol. 114, No. 32, 2010 **10281**

Figure 4. UV−vis absorption spectra of thin films of different P3HT/PMMA ratios. The P3HT/PMMA ratio of sample A is 1:5, sample B is 1:10, sample C is 1:50, sample D is 1:100, sample E is 1:500, and sample F is 1:1000.
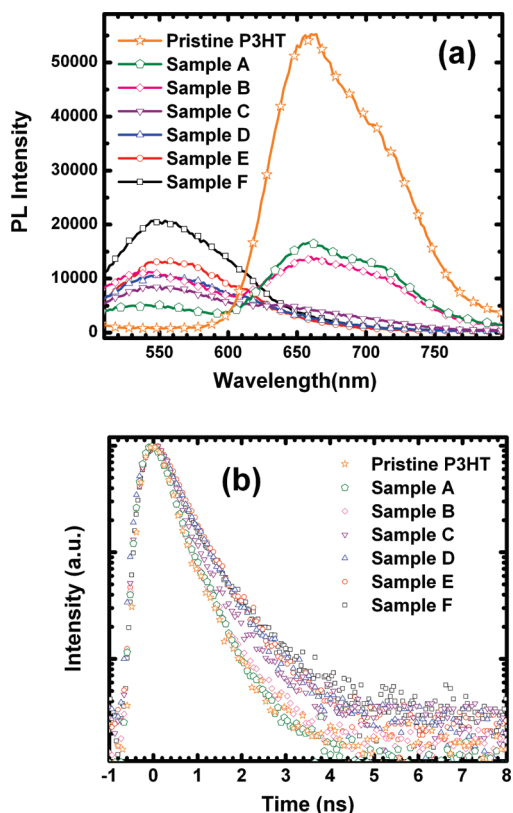

Figure 5. (a) Photoluminescence spectra of thin films with different P3HT/PMMA ratios. The ratios of P3HT/PMMA of sample A is 1:5, sample B is 1:10, sample C is 1:50, sample D is 1:100, sample E is 1:500, and sample F is 1:1000. (b) Time-resolved photoluminescence of the above samples at room temperature.

brighter color in the confocal microscope image correlates to increased signal captured by the single photon counting detector. Figure 6a,b shows that both sample A (1:5) and sample B (1:10) present an obvious photoluminescence from island-like domains. Recall that in the confocal Raman mapping image (Figure 3) the isolated domains are P3HT-rich regions while the continuous matrixes are PMMA-rich regions. Hence, the PL signals near 660 nm must come from the P3HT-rich island-like domains. However, when the blending ratio decreases, the confocal microscopic images of sample C (1:50) and sample D (1:100) show less color intensity over the films, meaning that a reduction in photoluminescence counts was collected. This matches the results of μ-PL spectra in Figure 5. Sample C (1:50) and sample D (1:100) show both weak peaks around 550

and 650 nm. When the blending ratios decrease to 1:500 and 1:1000, it is interesting to observe that both sample E (1:500) and sample F (1:1000) exhibit relatively higher PL intensity from the PMMA-rich regions than the P3HT-rich island-like domains as shown in Figure 6e,f. Since PMMA is nonconjugated polymer, the photoluminescence must emit from the P3HT polymer chains diluted in PMMA-rich regions. Such diluted P3HT surrounded by PMMA matrix emit a blue-shifted photoluminescence to around 550 nm as shown in sample E and sample F (Figure 5).

Figure 5b shows the TRPL measured at the wavelength with the strongest PL intensity, i.e., pristine P3HT, sample A (1:5), and sample B (1:10) at 660 nm and sample C (1:50), sample D (1:100), sample E (1:500), and sample F (1:1000) at 550 nm. According our previous work,[39] the measured lifetime of the luminescence τ_{PL} can be related to the rate constants of radiative and nonradiative decays k_R and k_{NR} and the radiative and nonradiative lifetime τ_R and τ_{NR} by

$$\frac{1}{\tau_{PL}} = \frac{1}{\tau_R} + \frac{1}{\tau_{NR}} = k_R + k_{NR} \qquad (1)$$

The photoluminescent efficiency is given by

$$\eta = f\frac{k_R}{k_R + k_{NR}} = f\frac{\tau_{PL}}{\tau_R} \qquad (2)$$

where f is the fraction of absorbed photons to emissive species. By exponentially fitting the PL lifetime decay curves, the obtained lifetimes of the luminescence τ_{PL} are listed in Table 2. In order to compare the radiative lifetimes at 660 nm that come from P3HT-rich regions, we designated the photoluminescent efficiency, i.e., PL intensity, and radiative lifetime of pristine P3HT as reference and denoted as 1 and τ_a, respectively. The radiative lifetimes of various blending ratios are then easily calculated and are summarized in Table 2. The obtained results are $1.00\tau_a$, $0.34\tau_a$, and $0.30\tau_a$ for pristine P3HT, sample A (1:5), and sample B (1:10), respectively. Similarly, for low blending ratios from 1:50 to 1:1000, we designated the photoluminescent efficiency and radiative lifetime of sample C (1:50) as reference and denoted as 1 and τ_b, respectively, as well, leading to radiative lifetimes $0.88\tau_b$, $0.75\tau_b$, and $0.48\tau_b$ for sample D (1:100), sample E (1:500), and sample F (1:1000), respectively. The results indicate that the radiative lifetimes monotonically decrease from τ_0 to $0.48\tau_b$ as the ratios decrease from 1:50 to 1:1000. On the basis of the faster radiative recombination rate and stronger PL intensity with increasing PMMA concentrations, we applied quantum well theory to deduce the mechanism of the PL blue shift. As the P3HT conjugated polymer chains are diluted in PMMA-rich domains, polymer chains would be isolated by the PMMA matrix. Therefore, PMMA can exercise a confinement effect on the P3HT and effectively suppress the energy transfer between small amounts of the well-separated conjugated P3HT polymer. The π electrons of the P3HT in PMMA are well localized and hop around in a way similar to that of P3HT oligomer rather than delocalized as in the pristine P3HT film. As a result, the effective conjugated length is reduced and the band gap is enlarged by quantum well approximation. Thus, a blue shift is observed in the PL spectrum of the film comprised of a low blending ratio.

Both the blending ratios and the molecular weight of P3HT have a great effect on the resolution of this novel resist.
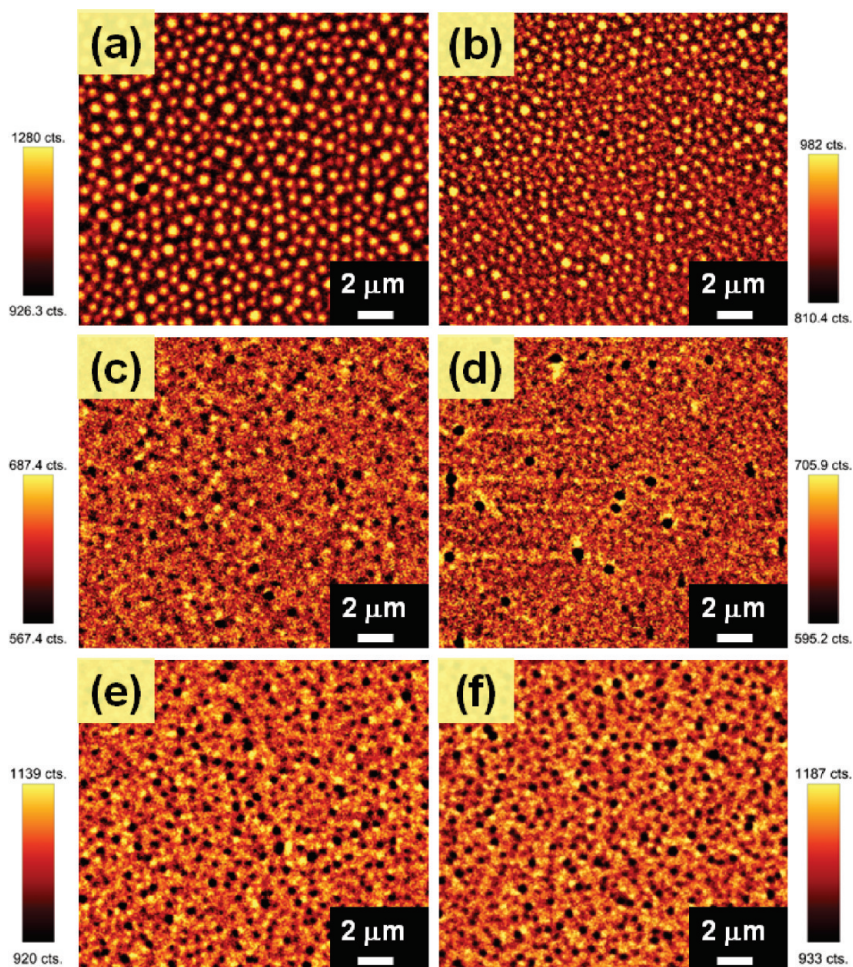
Figure 6. Confocal microscope images of thin films with different P3HT/PMMA ratios. The ratios of P3HT/PMMA are (a) sample A, 1:5; (b) sample B, 1:10; (c) sample C, 1:50; (d) sample D, 1:100; (e) sample E, 1:500; and (f) sample F, 1:1000.

TABLE 2: Summary of Measured PL Lifetime and the Relative Nature Radiative Lifetime for Pristine P3HT and P3HT/PMMA Films with Different Blending Ratios

sample	blending ratio (P3HT/PMMA)	τ_{PL} (ps)	τ_r λ_{max} at 660 nm	λ_{max} at 550 nm
pristine P3HT	1:0	380	τ_a	
A	1:5	415	$0.34\tau_a$	
B	1:10	420	$0.30\tau_a$	
C	1:50	450		τ_b
D	1:100	530		$0.88\tau_b$
E	1:500	530		$0.75\tau_b$
F	1:1000	530		$0.48\tau_b$

TABLE 3: Line Width Roughness of Different Photoluminescent P3HT/PMMA Resists

resist	MW of P3HT	PDI	P3HT:PMMA	σ_{LWR} (nm)
PMMA			0:1	4.1
resist A1	62 000	1.49	1:50	6.2
resist A2			1:100	6.0
resist A3			1:500	5.8
resist A4			1:1000	5.8
resist B1	33 800	1.32	1:50	6.0
resist B2			1:100	5.9
resist B3			1:500	5.8
resist B4			1:1000	5.7
resist C1	13 500	1.23	1:50	5.2
resist C2			1:100	5.1
resist C3			1:500	4.3
resist C4			1:1000	4.2

Therefore, we varied both factors respectively to examine the changes of the line width roughness σ_{LWR} of the patterned resist on flat silicon substrate. Table 3 shows the line width roughness, σ_{LWR}, of different P3HT/PMMA resists after electron beam lithography. We have seen that line width roughness increases with increasing P3HT/PMMA ratios in a fixed P3HT molecular weight. The large P3HT-rich domain in high blending ratios could hinder the electron beam lithography process; this decreases resolution. However, low molecular weight P3HT/PMMA electron beam resists (resist C series) exhibit better performance when compared with other higher molecular weights of P3HT in the resist (resist A series and resist B series). The lower molecular weight of P3HT carries shorter polymer chains and leads to smaller domains. The AFM images of the samples with 1:1000 blending ratio using different molecular weights of P3HT—13.5, 33.8, and 62.0 kDa—are shown in the Supporting Information. These images show that domain size decreases with decreasing the molecular weight of P3HT. The best P3HT/PMMA resist, resist C4, exhibits the lowest line width roughness of ~4.2 nm, which is close to that of the commercial PMMA electron beam resist (4.1 nm). As shown in the Table 3, the resist C4 also exhibits comparable surface roughness of commercial PMMA (0.78 and 0.67 nm).

The P3HT/PMMA resist denoted as resist C4 not only shows the desirable positive resist characteristics but also can be used to fabricate nanopatterns easily. Figure 7a–c shows the high-resolution field emission SEM images of periodic patterns made from resist C4 on a silicon substrate. Figure 7a is the SEM image
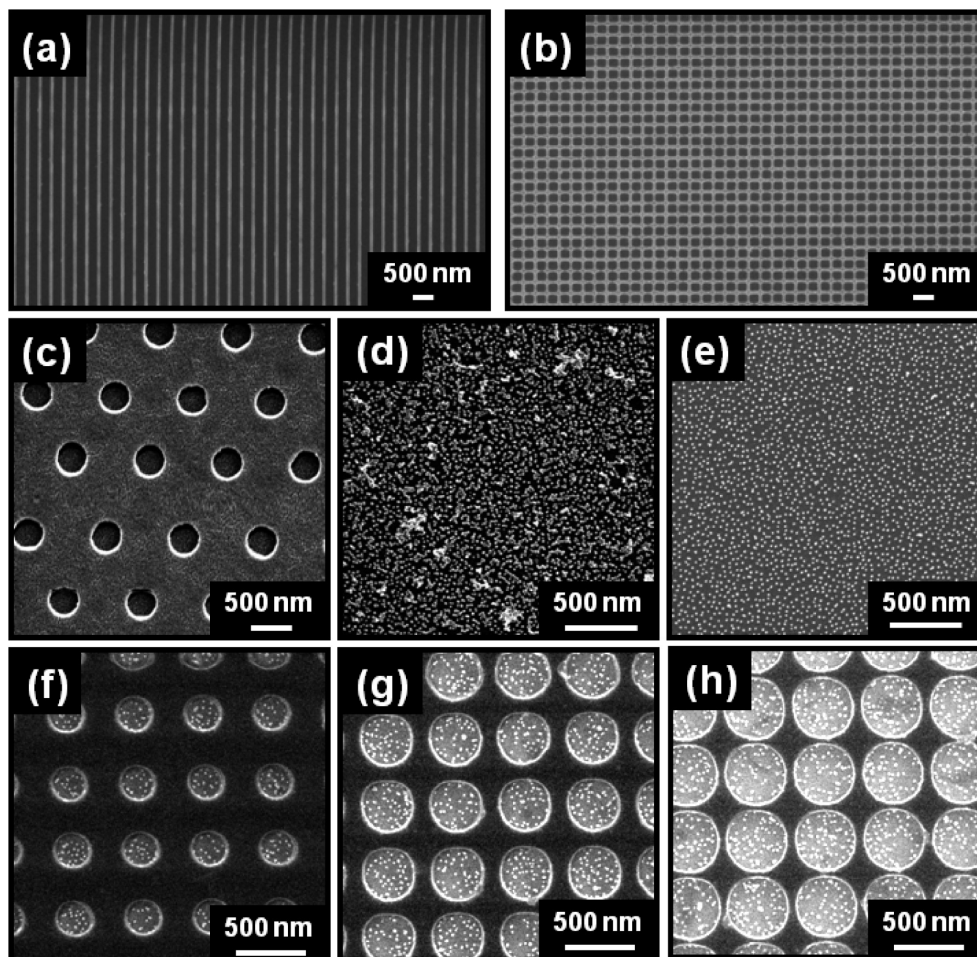
P3HT/PMMA Polymer Blends

J. Phys. Chem. B, Vol. 114, No. 32, 2010 **10283**

Figure 7. SEM images of patterned P3HT/PMMA on the silicon or Au NPs self-assembly substrate using resist C4. (a) Periodic lines with a width of 90 nm and an interval of 300 nm, (b) an array pattern with a width of 90 nm and an interval of 300 nm, (c) the P3HT/PMMA hole arrays with a lattice constant of 900 nm and a diameter of 370 nm, (d, e) Au nanoparticles self-assembled onto the APTMS/silicon substrate and the P3HT/PMMA periodic patterns with a lattice constant of 500 nm and different diameters, such as (f) 240 nm, (g) 390 nm, and (h) 440 nm, on the Au nanoparticles self-assembled substrate.
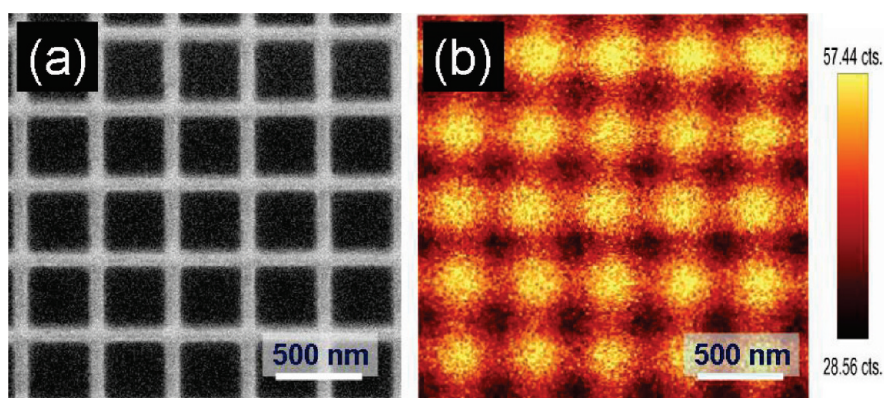

Figure 8. Periodic P3HT/PMMA arrays made from resist C4: (a) SEM image and (b) confocal reflect microscope image.

of straight lines with a width of 90 nm and an interval (distance between lines) of 300 nm. Figure 7b shows periodic square arrays exhibiting a width of 90 nm and interval of 300 nm. Figure 7c is the SEM image of the periodic P3HT/PMMA in a triangular style pattern with a lattice constant of 900 nm and the diameter of 370 nm. In addition to flat substrates such as silicon, we have also examined the resolution of our resist C4 using a rough substrate, i.e., Au NPs ∼20 nm self-assembled APTMS/silicon substrate since Au NPs are easy to aggregate on the APTMS/silicon substrate (Figure 7d). We were able to obtain a good Au 20 nm NPs self-assembled layer on APTMS/

silicon substrate as shown in Figure 7e by tuning the parameters such as immersion time and Au NP concentration. To confirm that various patterns can be easily fabricated using this electron beam PL resist on substrates with different surface profile, we made periodic hole arrays with square style pattern. These arrays were made from P3HT/PMMA resist with a lattice constant of 500 nm with varying diameters (240, 390, and 440 nm) on the Au nanoparticles self-assembled substrate, as shown in Figure 7f−h.

Figure 8a,b shows the SEM image and the confocal micros-copy image of the periodic arrays made from resist C4. From

the confocal microscopy images, we found that the film still exhibits photoluminescence after electron beam lithography, confirming that an electron beam resist with photoluminescent function was successfully developed. In this PL mapping measurement, we used an excitation filter to stimulate samples with an Ar ion laser at a wavelength of 488 nm. Finally, we compared the differences between P3HT and poly[2-methoxy-5(2-ethylhexyloxy)-*p*-phenylenevinylene (MEH-PPV) for the application of photoluminescent electron beam resist. Unfortunately, the resist made from MEH-PPV/PMMA was not excitable after the electron beam lithography. The results could be explained by thermogravimetric analysis, which is illustrated in the Supporting Information. It is apparent that the P3HT has better thermal stability than MEH-PPV because the P3HT could withstand the heating energy from an electron beam and still retain its PL properties. Therefore, simply blending P3HT and PMMA, we have obtained thermal stable PL electron beam resist that can be fabricated into photoluminescent nanopatterns.

4. Conclusions

It is found that the blending ratio of P3HT/PMMA film can control the domain size of the nanoscale phase separation which can significantly change the optical properties of the resist blends. Decreasing P3HT concentration produces a blue shift, longer PL lifetime, shorter radiative lifetime, and higher PL intensity. The results can be attributed to the confinement effect from the P3HT chains which are diluted and isolated in the PMMA-rich regions. By tuning the molecular weight of P3HT and blending ratios of P3HT/PMMA, we found that the resist made from the P3HT of 13 500 Da molecular weight at 1:1000 blending ratio exhibits a strong luminescence and high resolution with surface roughness of 0.67 nm and line width roughness of 4.2 nm. The patterns obtained from this resist could be well resolved not only on flat silicon substrate but also on rough substrate made by ∼20 nm Au nanoparticles on silicon. We have demonstrated that 2D photoluminescent spatial structures can be easily constructed by using this novel resist. Our new approach improves and expands the techniques for producing various future optoelectronic applications awaiting exploration.

Supporting Information Available: Atomic force microscope images and phase images of P3HT/PMMA blend thin films with different P3HT molecular weight (Figure S1) and TGA curves of conjugating polymer P3HT and MEH-PPV (Figure S2). This material is available free of charge via the Internet at http://pubs.acs.org.

References and Notes

(1) Bhuvana, T.; Subramaniam, C.; Pradeep, T.; Kulkarni, G. U. *J. Phys. Chem. C* **2009**, *113*, 7038.

(2) Bhuvava, T.; Gregoratti, L.; Heun, S.; Dalmiglio, M.; Kulkarni, G. U. *Langmuir* **2009**, *25*, 1259.

(3) Bhuvana, T.; Kulkarni, G. U. *Bull. Mater. Sci.* **2008**, *31*, 201.

(4) Saifullah, M. S. M.; Subramanian, K. R. V.; Kang, D.-J.; Anderson, D.; Huck, W. T. S.; Jones, G. A. C.; Welland, M. E. *Adv. Mater.* **2005**, *17*, 1757.

(5) Martiradonna, L.; Qualtieri, A.; Stomeo, T.; Carbone, L.; Cingolani, R.; Vittorio, M. D. *Sens. Actuators, A* **2007**, *126*, 116.

(6) Clendenning, S. B.; Aouba, S.; Rayat, M. S.; Grozen, D.; Sorge, J. B.; Broderson, P. M.; Sodhi, R. N. S.; Lu, Z. H.; Yip, C. M.; Freeman, M. R.; Ruda, H. E.; Manners, I. *Adv. Mater.* **2004**, *16*, 215.

(7) MacLachlan, M. J.; Ginzburg, M.; Coombs, N.; Coyle, T. W.; Raju, N. P.; Greedan, J. E.; Ozin, G. A.; Manners, I. *Science* **2000**, *287*, 1460.

(8) Clendenning, S. B.; Manners, I. *J. Vac. Sci. Technol. B* **2004**, *22*, 3493.

(9) Wu, M. C.; Chuang, M. C.; Lin, J. F.; Huang, Y. C.; Chen, Y. F.; Su, W. F. *J. Mater. Res.* **2009**, *24*, 394.

(10) Wu, M. C.; Wu, Y. J.; Huang, Y. C.; Chuang, C. M.; Cheng, K. C.; Lin, C. F.; Chen, Y. F.; Su, W. F. *J. Appl. Phys.* **2008**, *104*, 024517.

(11) Pang, L.; Shen, Y.; Tetz, K.; Fainman, Y. *Opt. Express* **2005**, *13*, 44.

(12) Song, J. H.; Atay, T.; Shi, S.; Urabe, H.; Nurmikko, A. V. *Nano Lett.* **2005**, *5*, 1557.

(13) Wu, M. C.; Chuang, C. M.; Lo, H. H.; Cheng, K. C.; Chen, Y. F.; Su, W. F. *Thin Solid Films* **2008**, *517*, 863.

(14) Li, Z. L.; Meng, H. F.; Horng, S. F.; Hsu, C. S.; Chen, L. C.; Chang, S. M. *Appl. Phys. Lett.* **2004**, *84*, 4944.

(15) Ananthakrishnan, N.; Padmanaban, G.; Ramakrishnan, S.; Reynolds, J. R. *Macromolecules* **2005**, *38*, 7660.

(16) Granström, M.; Inganäs, O. *Appl. Phys. Lett.* **1996**, *68*, 147.

(17) Luo, J.; Li, X.; Hou, Q.; Peng, J.; Yang, W.; Cao, Y. *Adv. Mater.* **2007**, *19*, 1113.

(18) Tasch, S.; List, E. J. W.; Ekström, O.; Graupner, W.; Leising, G.; Schlichting, P.; Rohr, U.; Geerts, Y.; Scherf, U.; Mü llen, K. *Appl. Phys. Lett.* **1997**, *71*, 2883.

(19) Zeng, T. W.; Lin, Y. Y.; Chen, C. W.; Su, W. F.; Chen, C. W.; Liou, S. H.; Huang, H. Y. *Nanotechnology* **2006**, *17*, 5387.

(20) Chen, L. C.; Inganäs, O.; Roman, L. S.; Johansson, M.; Andersson, M. *Thin Solid Films* **2000**, *363*, 286.

(21) McNeill, C. R.; Abrusci, A.; Zaumseil, J.; Wilson, R.; McKiernan, M. J.; Burroughes, H. J.; Halls, J. J. M.; Greenham, N. C.; Friend, R. H. *Appl. Phys. Lett.* **2007**, *90*, 193506.

(22) Lin, Y. J.; Li, Y. C.; Yeh, H. J.; Wang, Y. H.; Wen, T. C.; Huang, L. M.; Chen, Y. K. *Appl. Phys. Lett.* **2007**, *91*, 253501.

(23) Scott, J. C.; Jeyaprakash Samuel, J. D.; Hou, J. H.; Rettner, C. T.; Miller, R. D. *Nano Lett.* **2006**, *6*, 2916.

(24) Samuel, I. D. W.; Turnbull, G. A. *Chem. Rev.* **2007**, *107*, 1272.

(25) Berggren, M,; Inganäs, O.; Gustafsson, G.; Rasmusson, J.; Andersson, M. R.; Hjertnerg, T.; Wennerström, O. *Nature* **1994**, *372*, 444.

(26) Granström, M.; Inganäs, O. *Adv. Mater.* **1995**, *7*, 1012.

(27) McNeill, C. R.; Westenhoff, S.; Groves, C.; Friend, R. H.; Greenham, N. C. *J. Phys. Chem. C* **2007**, *111*, 19153.

(28) Iyenger, N. A.; Harrison, B.; Duran, R. S.; Schanze, K. S.; Reynolds, J. R. *Macromolecules* **2003**, *36*, 8978.

(29) Wu, M. C.; Liao, H. C.; Lo, H. H.; Chen, S.; Lin, Y. Y.; Yen, W. C.; Zeng, T. W.; Chen, C. W.; Chen, Y. F.; Su, W. F. *Sol. Energy Mater. Sol. Cells* **2009**, *93*, 961.

(30) Chou, H. L.; Hsu, S. Y.; Wei, P. K. *Polymer* **2005**, *46*, 4967.

(31) Wu, M. C.; Chang, C. H.; Lo, H. H.; Lin, Y. S.; Chen, C. W.; Yen, W. C.; Lin, Y. Y.; Chen, C. F.; Su, W. F. *J. Mater. Chem.* **2008**, *18*, 4097.

(32) Turkevich, J. *Gold Bull.* **1985**, *18*, 86.

(33) Chen, C. F.; Tzeng, S. D.; Lin, M. H.; Gwo, S. *Langmuir* **2006**, *22*, 7819.

(34) Cheng, W.; Dong, S.; Wang, E. *Chem. Mater.* **2003**, *15*, 2495.

(35) Flory, P. J. *J. Chem. Phys.* **1941**, *9*, 660.

(36) Huggins, M. L. *J. Chem. Phys.* **1941**, *9*, 440.

(37) Baibarac, M.; Lapkowski, M.; Pron, A.; Lefrant, S.; Baltog, I. *J. Raman Spectrosc.* **1998**, *29*, 825.

(38) Xu, X. *Opt. Commun.* **2001**, *199*, 89.

(39) Lin, Y. Y.; Chen, C. W.; Chang, J.; Lin, T. Y.; Liu, I. S.; Su, W. F. *Nanotechnology* **2006**, *17*, 1260.